e-VTOL Flying Test Bed

Technical Milestone Report

Samuel Drury

Supervised by: Dr Sam Grimshaw; Dr James Taylor

Introduction/Summary

Electric Vertical Take-Off and Landing (e-VTOL) vehicles are playing an increasingly important role in accelerating the path to zero-carbon flight, alongside bringing shorter commuting times at an affordable price. There is a choice to be made when selecting propulsors: while the simplicity of propellers make them an attractive option, the hovering performance and efficiency can be increased by using ducted fans, verified by previous work on propulsion systems for e-VTOL aircraft [1]. Additionally, the shrouding around the fans reduces the noise and brings an added safety benefit by shielding the rotating components. While work has been already conducted on selecting propulsors and assessing trade-offs in design, this has been limited to static tests on isolated propulsors. Developing a flying test bed allows the scope of experiments to be extended to explore dynamic performance and assess trade-offs for off-design conditions including crosswinds.

This report focuses on using an adapted design method to generate ducted fan blade profiles and quantify the increased performance over two different propellers. Following successful static tests, a set of four ducted fans are printed in Polylactic Acid (PLA) using an Ultimaker (3D printer) to develop a flying test bed (Fig. 1), whereby dynamic measurements can be taken to initially assess hover and stability performance.

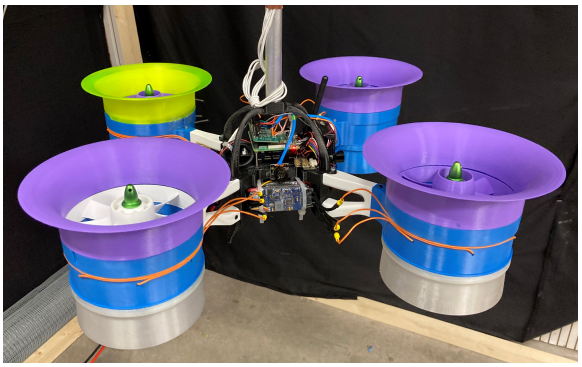

Figure 1: Flying test bed in hover

Design Method

2.1 Fan Design

The following methodology to design the ducted fans builds on work completed by previous students using MATLAB scripts further modified and refined by Dr Grimshaw.

2.1.1 Assumptions

In order to simplify the physics governing the fluid dynamics in the flow path, several assumptions are invoked that aid blade design. The flow is assumed to be incompressible and isentropic, and modelled to have no inlet or exit swirl; any swirl introduced to the flow by the rotor blades is removed by the stator blades. Additionally, the mean-line (not equal to 50% of the span due to a low hub-tip ratio) for the flow passage is calculated to ensure equal mass flow above and below (Eqn. 3.3).

2.1.2 Generating Blade Profiles

Appropriate values of flow coefficient ϕ and exit duct area ratio σ are selected from previous work[1], and used alongside the thrust requirement and geometry constraints.

Beginning with the Steady Flow Momentum and Energy equations, the axial velocity V_x and blade rotational speed Ω are determined. Next, the spanwise velocity distribution based on a mixed vortex design is determined, and using a stage loading coefficient for isentropic flow yields the flow angles. Lieblein's correlation[2] for diffusion factor sets the mean-line chord, which is used in Carter's empirical relation[3] to determine the meanline deviation, set to be constant across the span.

Now working backwards, a chord distribution that yields a constant deviation across the span is determined using Carter's rule again, and similarly Lieblein's correlation relates the chord distribution to the diffusion factor distribution, found to be below a preted-ermined threshold of 0.45, reducing the risk of stall. From the chord, diffusion factor and pitch (all at mean-line), the required number of blades for the rotor and stator is calculated.

Finally, to minimise end-wall losses and extend the propulsor operating range through limiting separation, suitable values of sweep and lean are selected from work by Taylor & Miller [4].

2.1.3 Design Point

Table 1 summarises the input parameters chosen for the final design, influenced by previous work on ducted fans [1], and the corresponding outputs. Note that the total thrust requirement with four propulsors is 51% greater than the flying test bed weight (26.5 N), and the RPM is suitably high to minimise the torque requirement from the motor and hence minimise the motor size.

Thrust	T_T	10 N
Hub radius	r_h	20 mm
Casing radius	r_c	60 mm
Exit area ratio	σ	1.13
Flow coefficient	ϕ	0.8
Stage loading	ψ	0.25
RPM	Ω	7900
FOM	M_f	1.50

Table 1: Summary of fan design point

2.2 3D Printing

DRAFT: I could talk about methodology, some notable points, design - is this necessary? This was something I didn't anticipate to get questioned on in the presentation, never mind be the only thing to get questioned on!

2.3 Determining Performance

2.3.1 Data Collection

Detailed descriptions for the methods of data collection are listed in the work done by a previous student [1]. In short, an on-board Raspberry Pi 3+ (RPi3+) module running Python scripts allows the RPM to be measured through an infra-red (IR) sensor and the thrust through a load cell (static test stand only), and this data is exported over WiFi using Secure Shell (SSH) protocol. A pressure transducer connected through Ethernet enables pressure readings to be taken from tappings along the ducted fan casing. Finally, the flight control hardware (Pixhawk 4) has accompanying software (QGroundControl) to control the fan(s), where a continuous feed including voltage and current measurements can be processed to obtain the input power.

2.3.2 Figure of Merit

When hovering, the conventional propulsive efficiency would equate to zero. As such, a new parameter is required to quantify the relative performance of different propulsors. Pereira[5] defines a Figure of Merit (FOM) as in Eqn. 2.1, which reduces to Eqn. 2.2 upon substitution for a ducted fan operating isentropically.

$$M_f = \frac{T_T}{P}\sqrt{\frac{T_T}{2\rho A_x}} \tag{2.1}$$

$$M_f = \sqrt{2\sigma} \tag{2.2}$$

2.3.3 Static tests with single ducted fan

Mounting the ducted fan or propeller to a fixed reference through a load cell allows the four measurements (RPM, thrust, pressures (ducted fan only) and power) to be taken, enabling the relative performance of propulsors to be quantified. Using QGroundControl, the fan speed can be varied to assess the variance of performance at different Reynold's numbers.

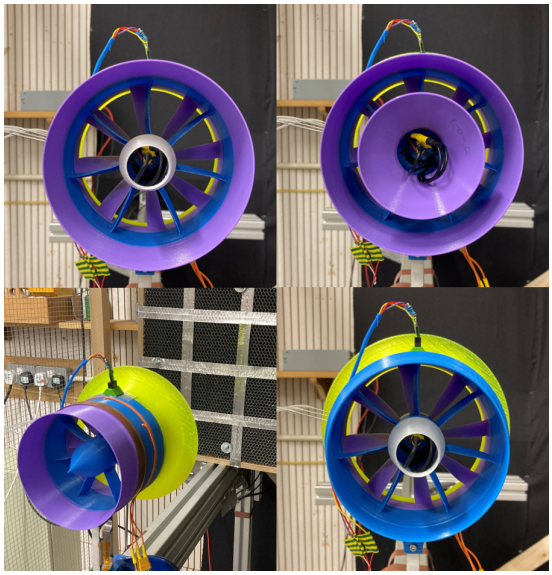

Figure 2: Varying exit area ratio, CW from top left: $\sigma = 1.13$ (design), 0.70, 0.89, 1.19 (with box fan at inlet)

The modular nature of the ducted fans means the exit area ratio (σ) can be varied by changing the inner and outer ducts, in an attempt to alter the operating point of the fan. A contracting duct limits the mass flow, reducing the flow coefficient ϕ and theoretically increasing the stage loading coefficient ψ, providing the fan hasn't stalled. On the other hand, diverging ducts increase the flow coefficient, and this can be further envisaged by placing a box fan upstream, along with a pitot tube to measure the new stagnation pressure, previously assumed to be atmospheric. Figure 2 displays four unique exit duct layouts used to obtain a characteristic for the ducted fan.

2.3.4 Dynamic tests with flying test bed

With four ducted fans mounted onto the chassis (Fig. 1), in-flight measurements can be taken remotely using the RPM IR sensor, casing pressure tappings, and the on-board Pixhawk 4 hardware with inbuilt accelerometers, gyros and ultrasound position sensors. Along with equating the ducted fan thrust to a quarter of the test bed weight, hover performance can be quantified, and the Pixhawk 4 sensor data can support conclusions of stability performance.

To progress beyond hover tests, pressures will have to be measured on the flying test bed, with data being exported over WiFi. This is feasible as up to three additional ADC breakout boards can be added to the RPi3+ to give a possible 30 ports for pressure sensors [6].

Experimental Results

3.1 Validating New Ducted Fan Design

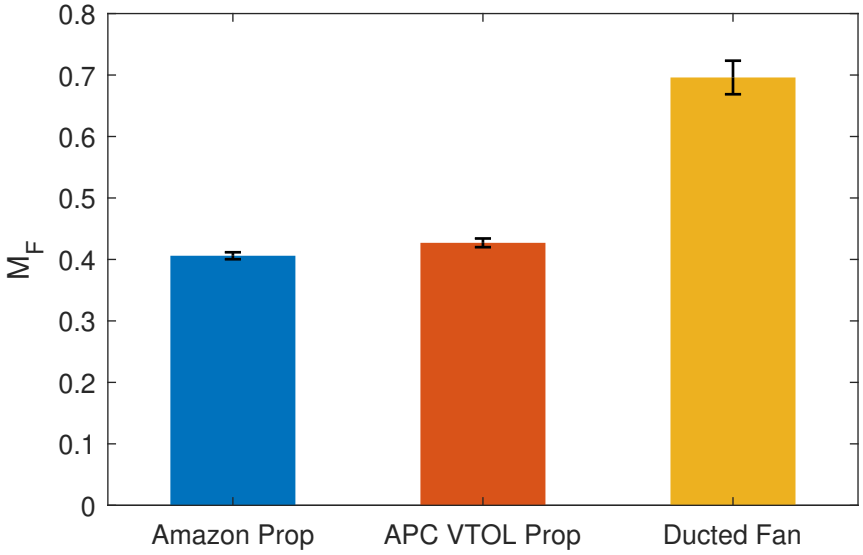

Figure 3: Comparing Figure of Merits for three different propulsors

Using measurements of thrust, RPM and input power (measured as Pixhawk 4 power consumption) from the static test stand, FOMs for three propulsors are shown in Fig. 3, where the error bars account for the variation in calculations for Reynolds numbers in the range 100,000 - 110,000. As expected, the Advanced Precision Composites (APC) VTOL-optimised propeller outperforms the cheaper stock propeller from Amazon by 5%, but the ducted fan is seen to have a FOM 63% greater. This not only validates the test stand, producing results agreeable with previous work[1], but justifies the importance of pursuing the development of ducted fans.

3.2 Characterising Ducted Fan

Figure 4 shows the mean line characteristic of the ducted fan, with non-dimensional pressure rise (stage loading/loading coefficient, ψ) plotted against non-dimensional mass flow rate (flow coefficient, ϕ). Equations 3.1 and 3.2 relate the values of ϕ and ψ calculated at the casing to the mean line using the vortex exponents A and B that satisfy radial equilibrium, and Fig. 5 highlights the pressure tapping locations.

Equation 3.4 relates the flow and loading coefficients to the exit area ratio for isentropic flow, and since the flow coefficient is set to be uniform at $\phi = 0.8$ across the span at inlet, this yields the theoretical design point. Due to flow irreversibilities arising from friction on the blade and hub/casing profiles, also resulting in lower momentum wakes forming from trailing edges, the actual design point has a lower loading coefficient.

Neglecting points where the flow stalls, a negative correlation is observed, which corroborates with typical compressor characteristics [7]. A key observation is that the design point has a comfortable stall margin, increasing stability for off-design conditions.

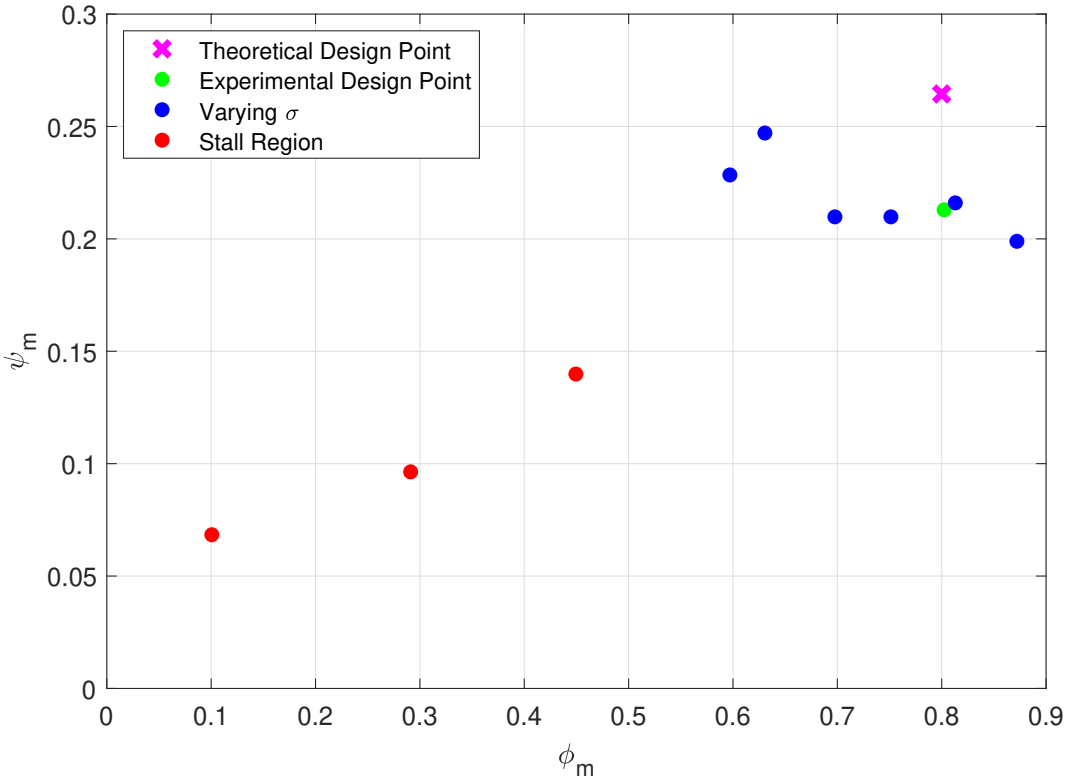

Figure 4: Ducted fan characteristic: loading coefficient vs flow coefficient

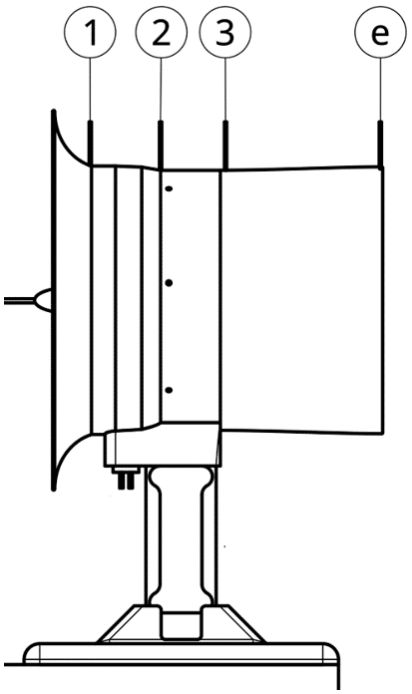

Figure 5: Static test stand with pressure tapping locations

$$\phi_m = \phi_c \left(\frac{r_c}{r_m}\right)^{-A}$$

$$\phi_m \approx \sqrt{\frac{(p_0 - p_1)_c}{\frac{1}{2}\rho(\Omega r_c)^2}} \cdot \left(\frac{r_c}{r_m}\right)^{-A} \tag{3.1}$$

$$\psi_c = \frac{(p_3 - p_0)_c}{\frac{1}{2}\rho(\Omega r_c)^2} + \frac{1}{2}\phi_c^2$$

$$\psi_m \approx \left[\frac{(p_3 - p_0)_c}{\frac{1}{2}\rho(\Omega r_c)^2} + \frac{1}{2}\phi_c^2\right] \cdot \left(\frac{r_c}{r_m}\right)^{-B} \tag{3.2}$$

$$r_m = \sqrt{\frac{r_h^2 + r_c^2}{2}} \tag{3.3}$$

$$\psi^2 = \frac{\phi^2}{2\sigma^2} \tag{3.4}$$

Conclusions

1. 3D printing is a suitable manufacturing method to produce propulsor designs generated through 1D and 2D fluid flow theory with added 3D features.
2. Ducted fans outperform propellers, with a 63% increase in Figure of Merit relative to a VTOL-optimised propeller.
3. Throttling a ducted fan by varying the exit area ratio is a successful method to obtain a fan characteristic. This helps validate the design theory and show there is a margin in the operating point before the fan stalls.
4. Using a previously developed modular flying test bed but now with ducted fans instead of propellers, successful test flights prove that measurements of performance and stability can be taken.

Future Work

In light of the UK lockdown beginning on 5th January 2021 due to the ongoing COVID-19 pandemic, restrictions on lab access render plans to continue developing the flying test bed infeasible at present. As such, the focus for the remainder of the project will centre on developing a loss model, accounting for: profile losses on the surface of blades; tip losses for leakage flow between the rotor shroud and casing wall; and end wall losses (hub and casing surfaces along the flow stream). The output will yield an aerodynamic efficiency that can be compared with CFD software Turbostream (Denton?). Using this model allows a multi-parameter optimisation to take place, taking potential inputs of: casing and hub diameters, exit area ratio, flow coefficient, vortex exponent and diffusion factor. As a result, trade-offs between properties such as: aerodynamic and propulsive efficiency, figure of merit, and tip Mach number can be realised, using the generated matrix of designs.

References

[1] J. Eriksen. “Propulsion Systems for VTOL Electric Vehicles” (2020).

[2] S. Lieblein, F. C. Schwenk, and R. L. Broderick. “Diffusion factor for estimating losses and limiting blade loadings in axial flow compressor blade elements.” *NACA R.M.* E53 D01 (1953).

[3] A. Carter. *The Low Speed Performance of Related Aerofoils in Cascade*. Current papers. Ministry of Supply, National Gas Turbine Establishment, 1950.

[4] J. Taylor and R. Miller. “Competing three-dimensional mechanisms in compressor flows” (2016).

[5] J. L. Pereira. “Hover and wind-tunnel testing of shrouded rotors for improved micro air vehicle design”. Tech. rep. (2008).

[6] ABelectronicsUK. *ADC Differential Pi*. URL: `https://www.abelectronics.co.uk/p/65/adc-differential-pi-raspberry-pi-analogue-to-digital-converter` (visited on 12/01/2021).

[7] S. L. Dixon and C. A. Hall. *Fluid Mechanics and Thermodynamics of Turbomachinery*. Seventh edition. Butterworth-Heinemann, 2014.